Group IV (Si, Ge, and Sn) Doped $AgAlTe_2$ for Intermediate Band Solar Cell from First-principles Study

Dan Huang[a, c], Jing-Wen Jiang[a], Jin Guo[a, c], Yu-Jun Zhao[b,*], Rong-Zhen Chen[d,e] and Clas Persson[d,e*]

a) Guangxi Key Laboratory for Relativistic Astrophysics, Guangxi Colleges and Universities Key Laboratory of Novel Energy Materials and Related Technology, College of Physics Science and Technology, Guangxi University, Nanning 530004, China
b) Department of Physics and State Key Laboratory of Luminescent Materials and Devices, South China University of Technology, Guangzhou 510640, China
c) Guangxi Collaborative Innovation Center of Structure and Property for New Energy and Materials, School of Material Science and Engineering, Guilin University of Electronic Technology, Guilin, China
d) Department of Physics, University of Oslo, PO Box 1048 Blindern, NO-0316 Oslo, Norway
e) Department of Materials Science and Engineering, Royal Institute of Technology, SE-100 44 Stockholm, Sweden

*Corresponding authors: zhaoyj@scut.edu.cn(Y.J.Z.); clas.persson@fys.uio.no(C.P.)

ABSTRACT: Earlier studies of chalcopyrites as the absorber for intermediate band solar cells (IBSC) mainly focused on Cu-based compounds, whose intermediate band is usually empty due to its intrinsic *p*-type conductivity. This is not beneficial to the two sub-band gap absorptions. In this paper, we demonstrate that the intermediate bands in group IV (Si, Ge and Sn) doped $AgAlTe_2$ are delocalized and mainly contributed by the anti-bonding state of group-IV elements *s* state and Te-*p* state. Overall, we suggest that Sn-doped $AgAlTe_2$ should be a promising absorber candidate for IBSC based on the theoretical efficiency and defect stability.

1. Introduction

The thin-film photovoltaic materials have drawn world-wide attention since converting sunlight into electricity is one of the most promising approaches to solve the energy and environment issues[1]. Chalcopyrite-structure (like $Cu(In,Ga)Se_2$) and its cousin kesterite-structure (like $Cu_2ZnSn(S,Se)_4$) materials as the absorber for the solar cells have been widely studied[2-5]. $Cu(In,Ga)Se_2$ and $Cu_2ZnSn(S,Se)_4$ thin-film photovoltaic devices have achieved a record efficiency of 22.3%[4] and 12.6%[5] on a laboratory scale, respectively. However, a thermodynamic analysis by Shockley and Queisser[6] shows that the efficiency of photovoltaic energy conversion of a single band gap solar cell is fundamentally limited to 31.0% at 1 sun concentration because of the broad spectral distribution of solar radiation, limiting the development space of thin-film solar cells. In 1997, the intermediate band solar cell (IBSC) concept [7-9] was proposed to overcome this limit for single band gap solar cells by making use of below band gap photons through sequential absorption processes via an intermediate band (IB). Luque and Martí[7] predicted that the efficiency in the IBSC could increase significantly over the Shockley-Queisser limit to 46.8% at 1 sun and 63.2% at full concentration[10]. The ideal width of the band gap for the IBSCs are 2.40 eV and 1.93 eV at 1 sun and full concentration [11,12], respectively.

Chalcopyrite-structure Cu-based compounds with a suitable band gap (like $CuGaS_2$[13-25], $CuAlSe_2$[26], $CuAlS_2$[27] *etc.*) as the promising host materials for IBSC have been investigated both theoretically and experimentally. From the experiments, distinct sub-gap absorptions related to the IB have been observed from Fe[13], Cr[14], Ti[15], Ge[16], and Sn[17] doped $CuGaS_2$ samples. The IB positions have been obtained from the absorption spectra measurements. Theoretically, Aguilera *et al.* [18] have investigated the electronic structures and optical properties of $Cu_4TiGa_3S_8$ and $Cu_4CrGa_3S_8$ by the generalized gradient approximation (GGA) calculations. Tablero [19] has investigated group-IV (C, Si, Ge, and Sn) doped $CuGaS_2$ by the local-spin density approximation (LDA) calculations. Both of them found the half-filled IB in the band gap and the increased absorption coefficient at the visible light range in their studied materials. More recently, hybrid functional like HSE(*i.e.* Heyd, Scuseria and Ernzerhof) was used to investigate the electronic structure and optical property of the IB absorber[17, 20-23], expecting more accurate description for the electronic properties (such as band gap, position of IB *etc.*) than the traditional LDA or GGA calculations. In fact, Hashemi *et al.* [20] found that the earlier reported half-filled IB had turned to be a lower filled and a higher empty sub-bands in Ti-substituted $CuGaS_2$ after adopting HSE06 functional. Meanwhile, Han *et al.*[21] found that unfilled IB appeared in the band gap in Fe and Co doped $CuGaS_2$, and

Yang *et al.* [17] found that there is still a half-filled IB in Sn-doped $CuGaS_2$ from HSE functional calculations. They also pointed out that the transition metal with localized 3*d* states might not be the best candidate to achieve high efficiently IB absorption in chalcopyrite compared to the group-IV element Sn with delocalized 5*s* state. From the electron dispersion point of view, the group-IV elements (Si, Ge and Sn) are the promising dopant candidates for IBSC. In order to obtain IBs in the gap, a large doping concentration is needed. In addition to electronic structure and optical property investigations, the free energy of formation and the allowed chemical potential derived from the first-principles calculations have been used to evaluate the possibility of doping concentration theoretically. From the investigation on the free energy of formation of the materials, Palacios *et al.* [24] found that the substitution by Cr or Ti at Ga sites in $CuGaS_2$ is energetically unfavorable, indicating that preparation methods controlled by kinetics must be used to obtain large dopant concentrations. To avoid the formation of impurities containing the doping elements, Tablero *et al.* [25] found that some of the elements (*i.e.* Fe, Co, Ni, Pd, Rh, Ir, Si, Ge, and Sn) can be soluble in $CuGaS_2$ and are suggested as the possible dopant candidates. Of note, they did not calculate the specific defect formation energies to find out the suitable doping element in detail.

As an absorber for the solar cell, Ag-based compounds have been paid

much less attention than the Cu-based compounds. Some of the Ag-based compounds (like $AgInSe_2$[28, 29], $AgGaTe_2$[30,31], $AgAlTe_2$[32], $Ag_2ZnSnSe_4$[33] *etc.*) have been reported for the applications on solar cells. On the other hand, Ag-based compounds have their unique properties with respect to the Cu-based compounds. Ag-based compounds generally have lower valence band position than Cu-based compounds [34, 35], implying that they are easier to be *n*-type[36]. For example, Yuan *et al.* [35] found from the first-principles study that the *p*-type defect Ag vacancy (V_{Ag}) in Ag_2ZnSnS_4 has much higher formation energy than Cu vacancy (V_{Cu}) in Cu_2CdSnS_4 and Cu_2ZnSnS_4. Experimentally, *n*-type conductivity has been reported in $AgInSe_2$[29] and $Ag_2ZnSnSe_4$[33]. Owing to the half-filled property required for IBs[37,38], the *p*-type conductivity in Cu-based compounds may lead to empty IB and this is destructive to the half-filled character of IB. Therefore, from the type of conductivity point of view, Ag-based compounds with a proper band gap may be more suitable as the host materials for IBSC. In addition, Ag-based chalcopyrite-type nanoparticles can be synthesized easily under milder reaction conditions than those of Cu-based ones[39]. Although Cu is cheaper and more abundant than Ag, Ag is advantageous with respect to In and Ga based on earth abundance and cost[40]. The inclusion of Ag in the thin film would not impose a large increase on the eventual cost of the solar panels[40]. The

chalcopyrite $AgAlTe_2$ with a band gap of 2.27 eV[41] has been investigated as the absorber for solar cells[32, 41] and the photo-catalyst for water splitting[42]. Its band gap is close to the ideal width (2.4 eV) for IBSC at 1 sun concentration. Therefore, $AgAlTe_2$ can be regarded as a promising host material for IBSC.

In this paper, group IV (Si, Ge, and Sn) doped $AgAlTe_2$ as an absorber for IBSC has been investigated by the first-principles study based on the HSE hybrid functional. Our results reveal that the IBs are dominated by the antibonding state of group-IV elements *s* state and Te-*p* state, which are more delocalized than that from transition metal doped chalcopyrite compounds. Based on the bond length and atomic orbital energy, we have explained the sequence of IBs in (Si, Ge and Sn)-doped $AgAlTe_2$. We also discuss the theoretical efficiency according to the width of sub-band gaps and evaluated the difficulty of doping to a large concentration based on the calculated defect formation energy. Our results show that Sn-doping at Al site in $AgAlTe_2$ has low formation energy under Te-rich condition and can produce the desired sub-band gaps for IBSC.

2. Computational details

All calculations were carried out by the density functional approach in the VASP package[43] with plane wave basis to describe the valence states. To describe the interactions between the valence electrons (Ag:

$4d^{10}5s^1$, Al: $3s^23p^1$, Te: $5s^25p^4$, Si: $3s^23p^2$, Ge: $4s^24p^2$, Sn: $5s^25p^2$) and the core, the projector augmented wave (PAW) implementation was used[44]. The calculations were performed using the screened hybrid exchange–correlation functional[45] developed by Heyd, Scuseria and Ernzerhof. The cutoff energy for the plane wave basis is set to 400 eV for all the calculations. In order to determine the IB position in the band gap without correction, the percentage of the exact non-local Fock exchange is adjusted to 30% to meet the accurate band gap of $AgAlTe_2$ from the experiment [41]. Our calculated crystal parameters for intrinsic $AgAlTe_2$ are $a = b$ = 6.38 Å, c = 12.11 Å, $c/2a$ =0.95, and u=0.27, in line with the experimental observations [46] ($a = b$ = 6.30 Å, c = 11.83Å, $c/2a$=0.94, and u= 0.26). For the calculations on systems containing defects, $\sqrt{2}\times\sqrt{2}\times1$ supercells containing 32 atoms (doping concentration at 12.5%) and 2×2×1 supercells containing 64 atoms (doping concentration at 6.25%) are adopted. For the calculation on defect formation energy, we used the supercells containing 64 atoms. All the atoms are fully relaxed throughout this work with the Γ-centered k-point mesh[47] of a reciprocal space discretization of ~0.17 $Å^{-1}$. After the structure relaxation, a denser Γ-centered k-mesh with a reciprocal space discretization of ~0.25 $Å^{-1}$ is used for the electronic structures and optical properties calculations.

3. Results and Discussions

Figure 1a and 1b show the total density of states (DOS) of the pure and (Si, Ge, and Sn)-doped $AgAlTe_2$ from 64-atoms supercells and 32-atoms supercells. We find that the DOSs of the valence and conduction bands do not show a significant change with and without doping. With Si, Ge, or Sn doped at Al site in $AgAlTe_2$, two series of additional peaks appear in the DOS. The first series of additional peaks (impurity peak I) are around the energy range from -8.5 to -7.2 eV on the sequence of Ge < Si < Sn. Another series of additional peaks (impurity peak II) are in the band gap, forming the IBs. The sequence of the IBs is Ge < Sn < Si. Since the two sub-gap absorptions are related to the position of the IB, it is important to understand the physics of the sequence, which has critical impact to the theoretical efficiencies of the doped systems.

The partials DOS(PDOS) of Si and Te in Si-doped $AgAlTe_2$ from 32-atoms supercell are shown in Figures 2a and 2b, from which we notice that the IB (i.e. the impurity peak II) mainly comes from the Si-*s* and Te-*p* states. In addition, the impurity peak I is also composed of Si-*s* state and Te-*p* state. To identify the bonding character of Si and Te, we have plotted their crystal orbital overlap populations (COOPs, see Figure 2c), which are computed using the Lobster program developed by Dronskowski and co-workers [48, 49]. The COOPs add the overlap dimension by showing the bonding (COOP > 0), non-bonding (COOP = 0)

or antibonding (COOP < 0) character of each electronic state over the system's chemical bonds. Combining the COOPs and PDOS, we can understand that the impurity peak I at around -9 eV comes from the bonding state of Si-*s* state and Te-*p* state and the IB (i.e. impurity peak II) in the band gap comes from the antibonding state of Si-*s* state and Te-*p* state. The wave function square (see figure 3a) of the IB in Si-doped $AgAlTe_2$ also shows the anti-bonding character, consistent with the bonding analysis from COOPs.

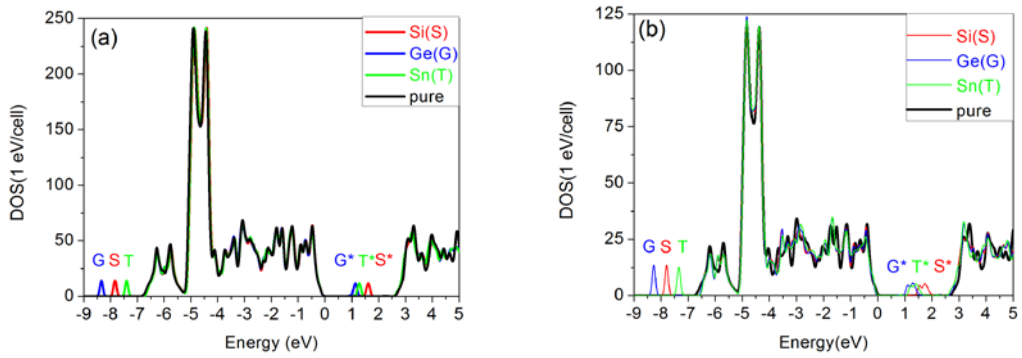

Figure 1. (Colour online) The total density of states of pure and (Si, Ge, and Sn)-doped $AgAlTe_2$ from 64-atoms supercells(a) and 32-atoms supercells(b). The average potentials of host elements far away from the dopant are used to align the DOS. The valence band maximum of the pure $AgAlTe_2$ is set to zero.

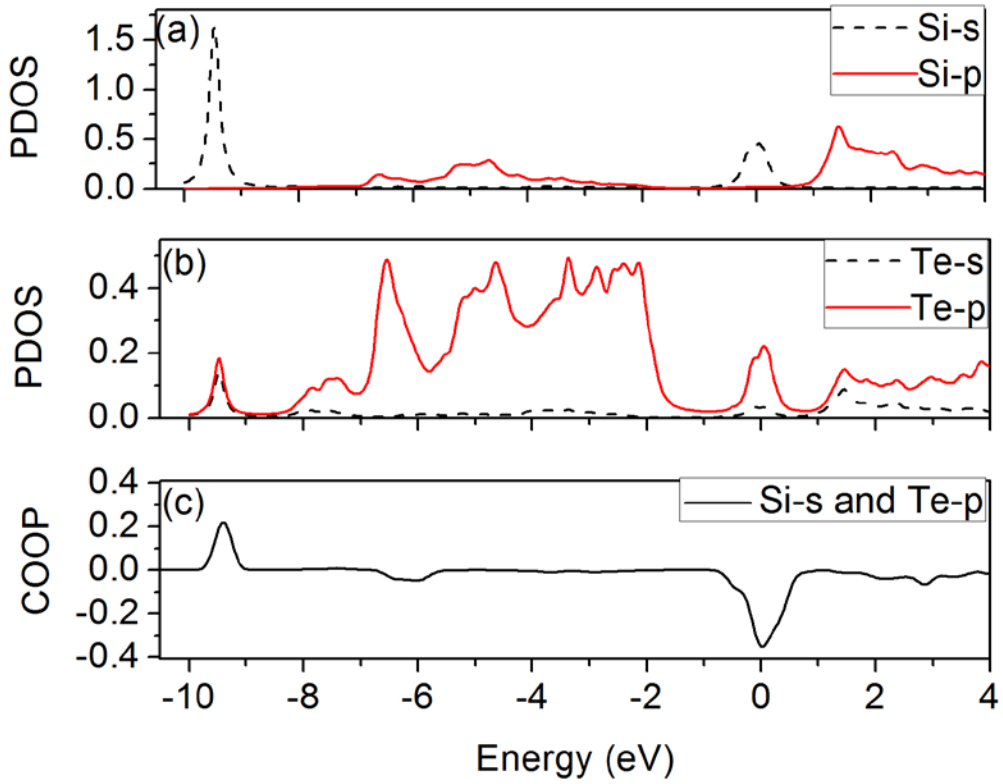

Figure 2. (Colour online) The partial density of state of Si(a) and Te(b) and the COOP(c) between Si-*s* and Te-*p* in Si-doped $AgAlTe_2$. The Fermi energy level is set to zero.

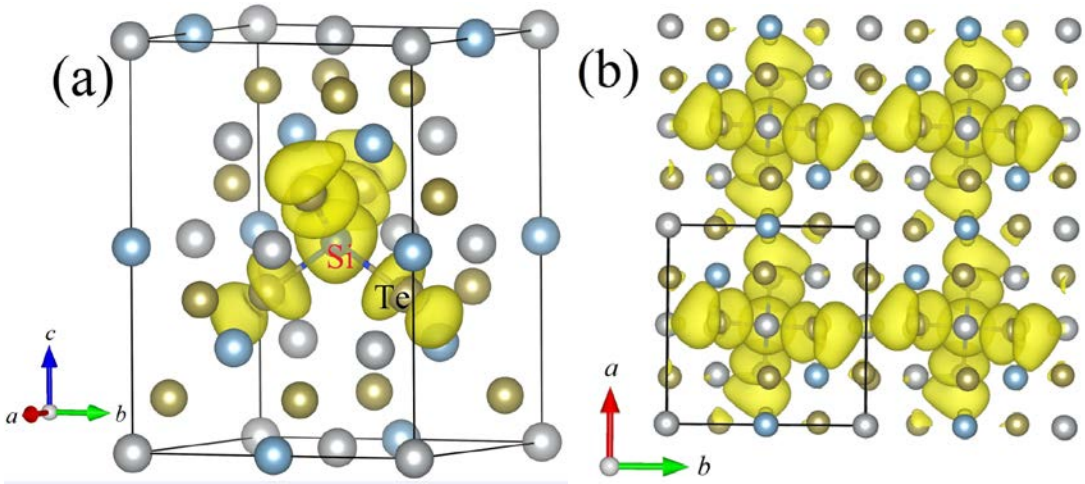

Figure 3. (Colour online) The wave function square of the IB in Si-doped $AgAlTe_2$. The densities are at 0.002 e/Å^3(a) and 0.001 e/Å^3(b), respectively.

For Ge and Sn-doped $AgAlTe_2$, the PDOS and bonding characters are similar with those of Si-doped $AgAlTe_2$. The atomic orbital energies [50] of Si-3*s*, Ge-4*s* and Sn-5*s* are -10.83, -11.61 and -10.05 eV, respectively. So the sequence of the energies of the outside *s*-electrons is Ge < Si < Sn, which is displayed in the left of Figure 4. The atomic orbital energy[50] of Te-5*p* is -6.17 eV, which is presented in the right of Figure 4. Beside the atomic orbital energy, the interactions between group-IV elements and Te are also influenced by the bond lengths. The calculated bond lengths of Si-Te, Ge-Te and Sn-Te in doped 32-atoms supercells are 2.67, 2.73 and 2.90 Å, respectively. Figure 4 shows the schematic diagram of the bonding/anti-bonding interactions between group-IV elements and Te in (Si, Ge, and Sn)-doped $AgAlTe_2$. Based on the atomic orbital energies and bond lengths, we can understand the sequence of the impurity peaks appeared in the DOS (Figure 1). Since Sn-*s* state has the highest atomic orbital energy and longest bond length, the bonding state of Sn-*s* and Te-*p* is at the highest position among all bonding states. Owing the shortest bond length of Si and Te and the mediate atomic orbital energy of Si-*s* state, the antibonding state of Si-*s* and Te-*p* is pushed to the highest position among all anti-bonding states. Due to the lowest atomic orbital energy of Ge-s and the mediate bond length of Ge and Te, the bonding/antibonding states of Ge-*s* and Te-*p* still stay at the lowest positions among the all bonding/anti-bonding states. Owing the IB

positions related to the sub-band gap absorption, the bonding analysis can provide a way to find a suitable dopant for the absorber of IBSC.

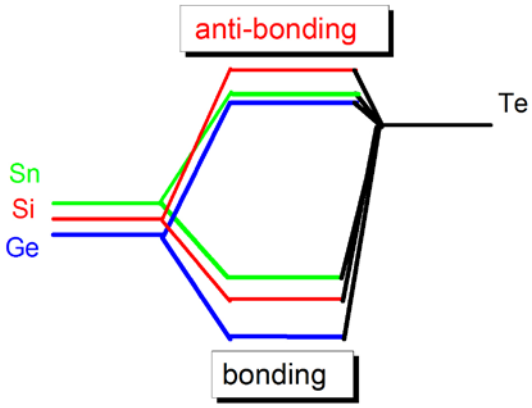

Figure 4. (Colour online) The schematic diagram of the bonding/ anti-bonding interactions of group-IV elements and Te in (Si, Ge and Sn)-doped $AgAlTe_2$.

When the doping concentration increases in $AgAlTe_2$, the original band gap and the width of the IB are expected to change correspondingly. We have calculated the band offsets among the pure and doped systems with different dopants for two different concentrations. The band offset was calculated with the conventional approach [51], *i.e.*, aligned by the average potentials of host elements far away from the dopant. Figure 5 presents the band offsets and schematic band structures for pure $AgAlTe_2$ and (Si, Ge and Sn)-doped $AgAlTe_2$ at two different doping concentrations. The width of the band gaps and the IBs are listed in Table 1. The original band gaps and the band edge positions are slightly influenced by doping. As expected, the width of the IBs broadens with the

increase of doping concentration. The width of the IBs increases from ~0.27-0.29 eV at the 6.25% doping concentration to ~0.75-0.78 eV at 12.5%，which are wider than those of the impurity bands from the transition metals doped chalcopyrite compounds (like $CuGaS_2$:Ti[20], $CuGaS_2$:Fe[22], $CuAlSe_2$:Ti[26] *etc.*) at the corresponding doping concentrations. The delocalized characters (see figure 3b) of the IBs in (Si, Ge and Sn)-doped $AgAlTe_2$ are originally from the group-IV *s* states and Te *p* states. Owing to the delocalized electronic structure of IBs, the generated carriers can transport freely and then overcome the non-radiative recombination[38, 52]. In addition, the impurity bands in transition metal doped chalcopyrite compounds are fully-filled or empty from previous HSE calculations[20, 21], which cannot serve the two-step jumping of an electron. The half-filled and delocalized properties of the IB of (Si, Ge and Sn)-doped $AgAlTe_2$ make them as the promising candidates for IBSC. Moreover, $AgAlTe_2$ is easier to maintain the Fermi level at *n*-type region to keep the IB half-filled than Cu-based chalcopyrite compounds.

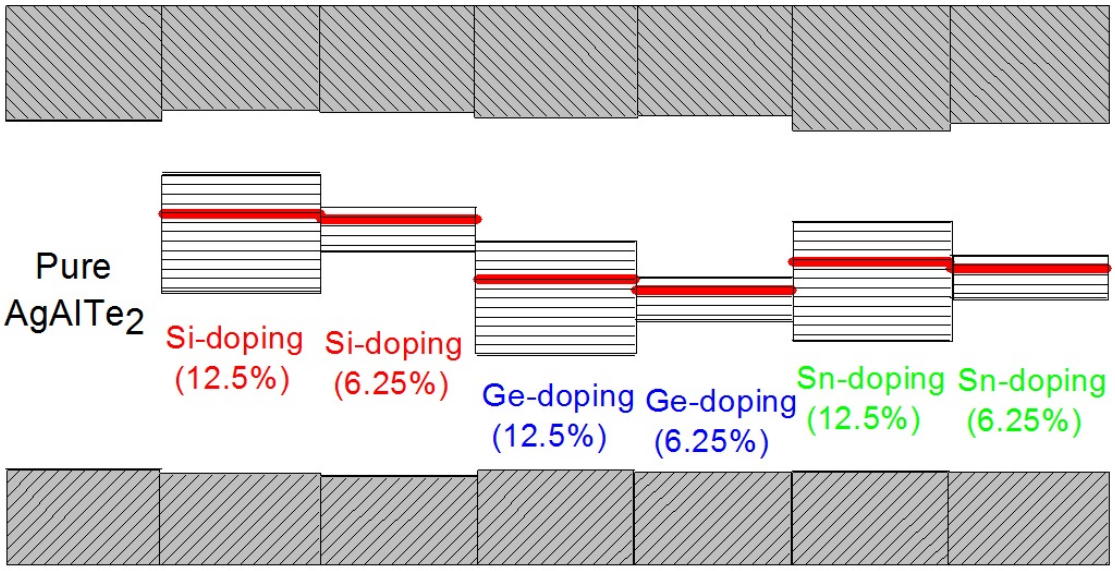

Figure 5. (Colour online) The band offsets and schematic band structures for pure $AgAlTe_2$ and group IV (Si, Ge and Sn) doped $AgAlTe_2$ at concentrations of 6.25% and 12.5%. The red lines in the IBs stand for the calculated Fermi level.

Table 1. The widths of band gap, sub-gap and IB (in eV), as well as the theoretical efficiency at 1 sun concentration in pure $AgAlTe_2$ and (Si, Ge and Sn)-doped $AgAlTe_2$ at doping concentrations of 6.25% and 12.5%.

Systems	Band gap	Sub-gap1 (VBM-Fermi)	Sub-gap2 (Fermi-CBM)	Width of IB	Theoretical efficiency at 1 sun concentration
Pure-$AgAlTe_2$	2.27				23%
Si (12.5%)	2.39	1.70	0.69	0.78	38%
Si (6.25%)	2.38	1.68	0.70	0.29	39%
Ge (12.5%)	2.33	1.26	1.07	0.75	33%
Ge (6.25%)	2.33	1.19	1.14	0.27	24%
Sn (12.5%)	2.24	1.37	0.87	0.78	45%
Sn (6.25%)	2.29	1.34	0.95	0.28	41%

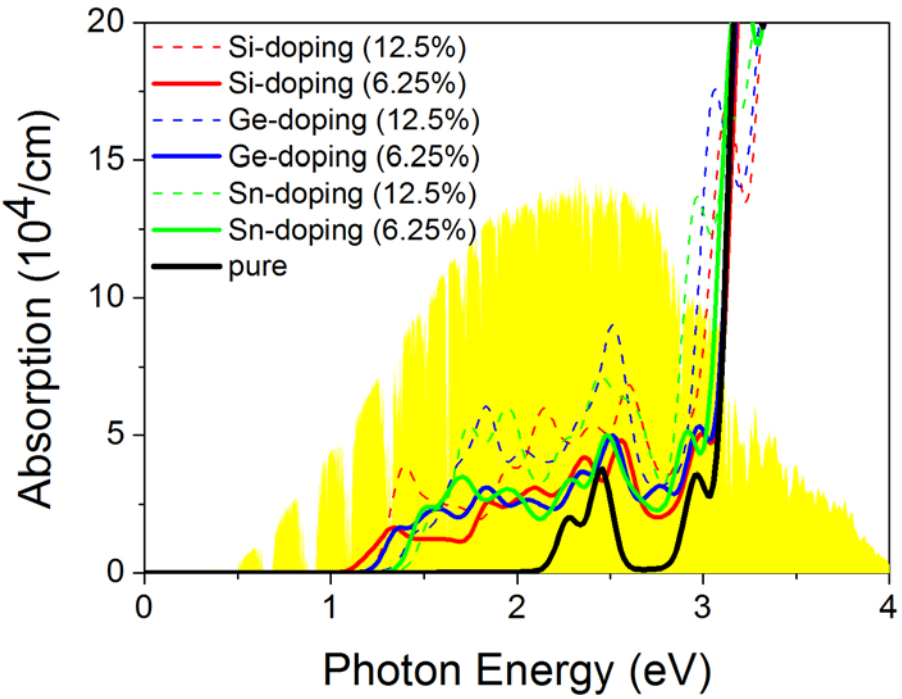

Figure 6. (Colour online) The absorption coefficient of pure $AgAlTe_2$ and (Si, Ge and Sn)-doped $AgAlTe_2$ with two different concentrations. The reference air-mass 1.5-solar spectral irradiance is plotted in yellow.

Figure 6 presents the absorption coefficient of pure $AgAlTe_2$ and (Si, Ge and Sn)-doped $AgAlTe_2$ at doping concentrations of 6.25% and 12.5%. Obviously, the capabilities of light absorption have been enhanced for the doped systems under the solar radiation spectrum by the sub-band gap absorption. With the doping concentration increases from 6.25% to 12.5%, the absorption coefficient is also improved. Based on the width of the band gap and the sub-band gap listed in Table 1, we estimate the theoretical efficiency at 1 sun concentration of each our studied materials. Owing to the similar width of the two sub-band gaps (for example, 1.19

and 1.14 eV for Ge doping at 6.25% concentration), Ge-doped $AgAlTe_2$ has the lowest theoretical efficiency among the (Si, Ge, and Sn)-doped $AgAlTe_2$. For Si and Sn doped $AgAlTe_2$, the theoretical efficiency at 1 sun concentration can increase to ~40% owing to the appropriate sub-band gaps. Especially for Sn doping at 12.5% concentration, the theoretical efficiency can reach up to 45%, which is close to the maximum theoretical efficiency (46.8%) of an absorber with one IB at 1 sun concentration [10].

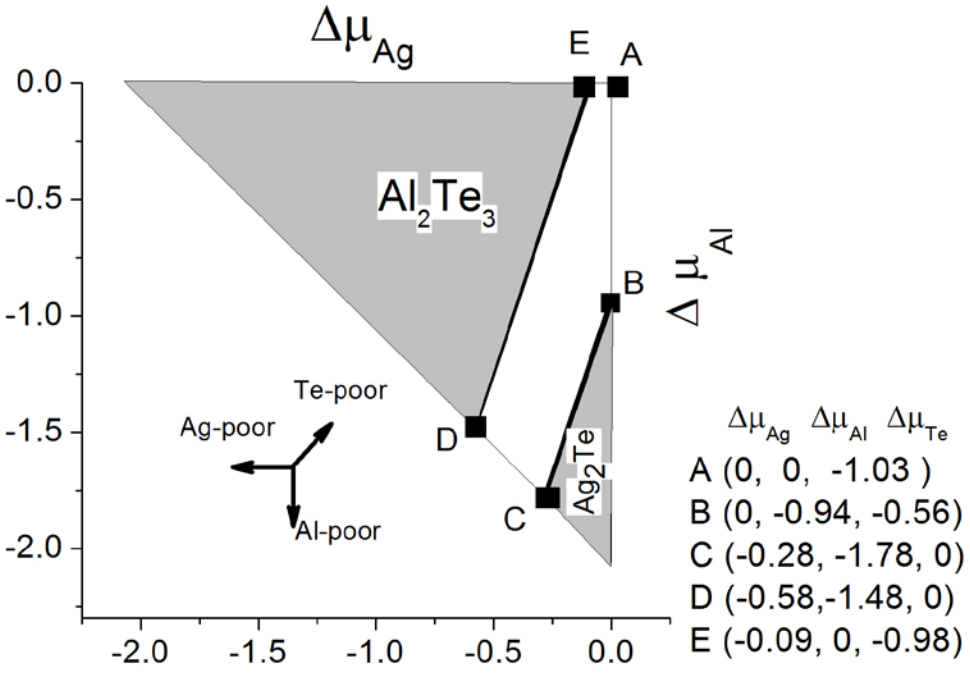

Figure 7. The allowed chemical potential ranges (white area in the triangle) for a stable $AgAlTe_2$ with consideration of competing compounds. Points A, B, C, D and E represent five extreme conditions considered in this work.

In order to obtain an IB other than impurity level in the doped systems, the samples generally need to contain dopants with a large concentration. To evaluate the possibility to reach a large concentration of group IV dopants in $AgAlTe_2$, we have calculated the defect formation energy [53] according to:

$$\Delta E(D^0) = E(D^0) - E(0) + \sum_{\alpha} n_{\alpha}(\Delta\mu_{\alpha} + \mu_{\alpha}^{solid}) \quad (1).$$

where $E(D^0)$ and $E(0)$ are the total energies of the supercells with and without defects. Here ($\Delta\mu_{\alpha}$+ $\mu^{\text{solid}}{}_{\alpha}$) is the absolute value of the chemical potential of atom α. $\mu^{\text{solid}}{}_{\alpha}$ is defined as the chemical potential of the elemental solid. Also n_{α} is the number of atoms related to the defect; n_{α}= −1 if an atom is added, while n_{α}= 1 if an atom is removed.

The chemical potentials of each constituent species ($\Delta\mu_{\alpha}$) can be varied to reflect specific equilibrium growth conditions, but their summation is always equal to the calculated formation enthalpy of $AgAlTe_2$ in order to maintain the stability of the host:

$$\Delta\mu_{\text{Ag}} + \Delta\mu_{\text{Al}} + 2\Delta\mu_{\text{Te}} = \Delta\text{H}(AgAlTe_2) = -2.06 \text{ eV} \quad (2).$$

In addition to the host stability condition, the atomic chemical potentials should be smaller than that of the corresponding elemental solid in order to avoid precipitation of elemental solids:

$$\Delta\mu_{\text{Ag}} \leq 0,\ \Delta\mu_{\text{Al}} \leq 0,\ \Delta\mu_{\text{Te}} \leq 0 \quad (3).$$

The chemical potentials are further restricted by the competing compounds. These crucial constraints are listed as the following:

$$2\Delta\mu_{Al} + 3\Delta\mu_{Te} \leq \Delta H(Al_2Te_3) = -2.96 \text{ eV} \quad (4).$$

$$2\Delta\mu_{Ag} + \Delta\mu_{Te} \leq \Delta H(Ag_2Te) = -0.56 \text{ eV} \quad (5).$$

Figure 7 shows the calculated chemical potential domains for $AgAlTe_2$. From the constraints imposed by the competing compounds, the white areas in the triangle are the allowed chemical potential ranges for $AgAlTe_2$. Within this boundary, we explicitly consider five extreme growth conditions. The detailed values of the chemical potentials of Ag, Al and Te under different growth conditions are shown in figure 7. The maximum allowed values of the chemical potentials for Si, Ge and Sn are used for the defect formation calculations, with the following constrains: $2\Delta\mu_{Si}+3\Delta\mu_{Te} \leq \Delta H(Si_2Te_3) = -0.80$ eV, $\Delta\mu_{Ge}+\Delta\mu_{Te} \leq \Delta H(GeTe) = -0.20$ eV, $\Delta\mu_{Sn}+\Delta\mu_{Te} \leq \Delta H(SnTe) = -0.15$ eV. Here the experimental data of the formation enthalpies of Si_2Te_3[54], GeTe[55] and SnTe[56] are adopted.

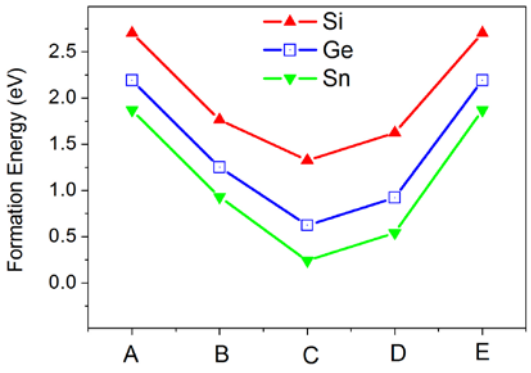

Figure 8. (Colour online) The formation energies of Si, Ge and Sn substituting at Al site in $AgAlTe_2$ as a function of the chemical potential at points A, B, C, D and E shown in Fig. 7.

Figure 8 shows the formation energies of Si, Ge and Sn substituting at Al site in $AgAlTe_2$ under various chemical potential conditions. We find that Sn doping always has the lowest formation energy compared to Si and Ge doping and can reach to 0.24 eV under C point (i.e. Te-rich condition), which implies that Sn_{Al} can reach to a large doping concentration. Using the Boltzmann distribution law and assuming the growth temperature T of 1000K [32], the Sn_{Al} doping concentration can reach to ~6% under Te-rich condition. As we mentioned before, our calculated defect formation energies are based on using the elemental solid as the dopant source under equilibrium condition. By using other dopant sources [57] (like SiH_4, GeH_4 *etc.*) and the non-equilibrium growth method [58], the doping concentration may further increase in Si or Ge doped $AgAlTe_2$ to break up the limit of the equilibrium doping. These methods can also be utilized to achieve a large Sn doping concentration. Combining the theoretical efficiency and defect formation energy, we suggest that Sn doped $AgAlTe_2$ can realize a large doping concentration easily and possess a desired theoretical efficiency, which should be a promising absorber candidate for IBSC.

4. Conclusion

In summary, we have studied the (Si, Ge and Sn)-doped $AgAlTe_2$ as an absorber for IBSC by the HSE hybrid functional calculation. Our results

indicate that all the studied dopants can induce a delocalized IB in $AgAlTe_2$, dominated by the anti-bonding state of group-IV element *s* and Te-*p* states. The energy sequence of the IB positions in the band gap is Ge < Sn < Si, which can be explained by the bond lengths and atomic orbital energies. Based on the width of the sub-band gap and the defect formation energy, we have evaluated the theoretical efficiency and the possibility of doping with a large concentration. The results suggested that Sn-doped $AgAlTe_2$ can achieve a high theoretical efficiency and realize a large doping concentration, which is regarded as a promising absorber for IBSC.

Acknowledgments

This work was financially supported by the National Natural Science Foundation of China (Grant Nos. 61664003, 51571065, and 11574088), the Natural Science Foundation of Guangxi Province (Grant Nos. 2014GXNSFCA118002), the Scientific Research Foundation of Guangxi University (Grant No. XGZ130718), and the Research Council of Norway (Grant No. 243642). We acknowledge usage of supercomputer resources at Barcelona Supercomputing Center (BSC).

Reference:

1. Polman A, Knight M, Garnett E C, et al. Photovoltaic materials: Present efficiencies and future challenges[J]. Science, 2016, 352(6283): aad4424.
2. Contreras M A, Egaas B, Ramanathan K, et al. Progress toward 20% efficiency in Cu(In,Ga)Se_2 polycrystalline thin-film solar cells[J]. Progress in Photovoltaics: Research and applications, 1999, 7(4): 311-316.
3. Todorov T K, Tang J, Bag S, et al. Beyond 11% efficiency: characteristics of state-of-the-art $Cu_2ZnSn(S,Se)_4$ solar cells[J]. Advanced Energy Materials, 2013, 3(1): 34-38.
4. Jackson P, Wuerz R, Hariskos D, et al. Effects of heavy alkali elements in Cu(In, Ga)Se_2 solar cells with efficiencies up to 22.6%[J]. Physica Status Solidi (RRL)-Rapid Research Letters, 2016, 10(8): 583-586.
5. Wang W, Winkler M T, Gunawan O, et al. Device characteristics of CZTSSe thin-film solar cells with 12.6% efficiency[J]. Advanced Energy Materials, 2014, 4(7).
6. Shockley W, Queisser H J. Detailed balance limit of efficiency of p-n junction solar cells[J]. Journal of Applied Physics, 1961, 32(3): 510-519.
7. Luque A, Martí A. Increasing the efficiency of ideal solar cells by photon induced transitions at intermediate levels[J]. Physical Review Letters, 1997, 78(26): 5014.
8. Luque A, Martí A, Stanley C. Understanding intermediate-band solar cells[J]. Nature Photonics, 2012, 6(3): 146-152.
9. Okada Y, Ekins-Daukes N J, Kita T, et al. Intermediate band solar cells: Recent progress and future directions[J]. Applied Physics Reviews, 2015, 2(2): 021302.
10. Brown A S, Green M A. Impurity photovoltaic effect: Fundamental energy conversion efficiency limits[J]. Journal of Applied Physics, 2002, 92(3): 1329-1336.
11. Ley M, Boudaden J, Kuznicki Z T. Thermodynamic efficiency of an intermediate band photovoltaic cell with low threshold Auger generation[J]. Journal of Applied Physics, 2005, 98(4): 044905.
12. Wang W, Lin A S, Phillips J D. Intermediate-band photovoltaic solar cell based on ZnTe: O[J]. Applied Physics Letters, 2009, 95(1): 011103.
13. Marsen B, Klemz S, Unold T, et al. Investigation of the sub-bandgap photoresponse in $CuGaS_2$:Fe for intermediate band solar cells[J]. Progress in Photovoltaics: Research and Applications, 2012, 20(6): 625-629.
14. Chen P, Qin M, Chen H, et al. Cr incorporation in $CuGaS_2$ chalcopyrite: A new intermediate-band photovoltaic material with wide-spectrum solar absorption[J]. Physica Status Solidi (a), 2013, 210(6): 1098-1102.
15. Lv X, Yang S, Li M, et al. Investigation of a novel intermediate band photovoltaic material with wide spectrum solar absorption based on Ti-substituted $CuGaS_2$[J]. Solar Energy, 2014, 103: 480-487.
16. Qin M S, Huang F Q, Chen P. Wide spectrum absorption of $CuGaS_2$ with intermediate bands[C] Applied Mechanics and Materials, 2012, 148: 1558-1561.
17. Yang C, Qin M, Wang Y, et al. Observation of an intermediate band in Sn-doped

chalcopyrites with wide-spectrum solar response[J]. Scientific Reports, 2013, 3:1286.
18. Aguilera I, Palacios P, Wahnón P. Enhancement of optical absorption in Ga-chalcopyrite-based intermediate-band materials for high efficiency solar cells[J]. Solar Energy Materials and Solar Cells, 2010, 94(11): 1903-1906.
19. Tablero C. Electronic and optical properties of the group IV doped copper gallium chalcopyrites[J]. Thin Solid Films, 2010, 519(4): 1435-1440.
20. Hashemi J, Akbari A, Huotari S, et al. Multi-intermediate-band character of Ti-substituted $CuGaS_2$: Implications for photovoltaic applications[J]. Physical Review B, 2014, 90(7): 075154.
21. Han M, Zhang X, Zeng Z, The investigation of transition metal doped $CuGaS_2$ for promising intermediate band materials[J]. RSC Advances, 2014, 4(107), 62380-62386.
22. Koskelo J, Hashemi J, Huotari S, et al. First-principles analysis of the intermediate band in $CuGa_{1-x}Fe_xS_2$[J]. Physical Review B, 2016, 93(16): 165204.
23. Han M, Zhang X, Zhang Y, et al. The group VA element non-compensated n–p codoping in $CuGaS_2$ for intermediate band materials[J]. Solar Energy Materials and Solar Cells, 2016, 144: 664-670
24. Tablero C, Fuertes Marrón D. Analysis of the electronic structure of modified $CuGaS_2$ with selected substitutional impurities: prospects for intermediate-band thin-film solar cells based on Cu-containing chalcopyrites[J]. The Journal of Physical Chemistry C, 2010, 114(6): 2756-2763.
25. Palacios P, Aguilera I, Wahnón P, et al. Thermodynamics of the formation of Ti-and Cr-doped $CuGaS_2$ intermediate-band photovoltaic materials[J]. The Journal of Physical Chemistry C, 2008, 112(25): 9525-9529.
26. Wang T, Li X, Li W, et al. Transition metals doped $CuAlSe_2$ for promising intermediate band materials[J]. Materials Research Express, 2016, 3(4): 045905.
27. Guo C, Yang C, Xie Y, et al. Preparation of Sn-doped $CuAlS_2$ films with an intermediate band and wide-spectrum solar response[J]. RSC Advances, 2016, 6(47): 40806-40810.
28. Mustafa H, Hunter D, Pradhan A K, et al. Synthesis and characterization of $AgInSe_2$ for application in thin film solar cells[J]. Thin Solid Films, 2007, 515(17): 7001-7004.
29. Jacob R, Okram G S, Naduvath J, et al. Tin Incorporation in $AgInSe_2$ thin films: influence on conductivity[J]. The Journal of Physical Chemistry C, 2015, 119(10): 5727-5733.
30. Krustok J, Jagomägi A, Grossberg M, et al. Photoluminescence properties of polycrystalline $AgGaTe_2$[J]. Solar Energy Materials and Solar Cells, 2006, 90(13): 1973-1982.
31. Kumar R, Bedi R K. Characterization of thermally evaporated $AgGaTe_2$ films grown on KCl substrates[J]. Journal of Materials Science, 2005, 40(2): 455-459.
32. Uruno A, Usui A, Kobayashi M. Growth of $AgGaTe_2$ and $AgAlTe_2$ layers for novel photovoltaic materials[J]. Journal of Electronic Materials, 2014, 43(8): 2874-2878.
33. Gershon T, Sardashti K, Gunawan O, et al. Photovoltaic device with over 5%

efficiency based on an n-Type $Ag_2ZnSnSe_4$ absorber[J]. Advanced Energy Materials, 2016, 6(22): 1601182.
34. Huang D, Persson C. Photocatalyst $AgInS_2$ for active overall water-splitting: A first-principles study[J]. Chemical Physics Letters, 2014, 591: 189-192.
35. Yuan Z K, Chen S, Xiang H, et al. Engineering solar cell absorbers by exploring the band alignment and defect disparity: The case of Cu- and Ag-Based kesterite compounds[J]. Advanced Functional Materials, 2015, 25(43): 6733-6743.
36. Zhang S B, Wei S H, Zunger A. Microscopic origin of the phenomenological equilibrium “doping limit rule” in n-type III-V semiconductors[J]. Physical Review Letters, 2000, 84(6): 1232.
37. Luque A, Marti A. A metallic intermediate band high efficiency solar cell[J]. Progress in Photovoltaics: Research and Applications, 2001, 9(2): 73-86.
38. Zhang J, He H, Pan B. Fe/Co doped molybdenum diselenide: a promising two-dimensional intermediate-band photovoltaic material[J]. Nanotechnology, 2015, 26(19): 195401.
39. Torimoto T, Kameyama T, Kuwabata S. Photofunctional materials fabricated with chalcopyrite-type semiconductor nanoparticles composed of $AgInS_2$ and its solid solutions[J]. The Journal of Physical Chemistry Letters, 2014, 5(2): 336-347.
40. Chagarov E, Sardashti K, Kummel A C, et al. $Ag_2ZnSn(S,Se)_4$: A highly promising absorber for thin film photovoltaics[J]. The Journal of chemical physics, 2016, 144(10): 104704.
41. Uruno A, Takeda Y, Inoue T, et al. Crystallographic and optical characterizations of $Ag(Ga,Al)Te_2$ layers grown on c-plane sapphire substrates by closed space sublimation[J]. Physica Status Solidi (c), 2016, 13: 413-416.
42. Huang D, Ju Z, Ning H, et al. First-principles study on $CuAlTe_2$ and $AgAlTe_2$ for water splitting[J]. Materials Chemistry and Physics, 2014, 148(3): 882-886.
43. Kresse G, Hafner J. Ab initio molecular dynamics for liquid metals[J]. Physical Review B, 1993, 47(1): 558.
44. Kresse G, Joubert D. From ultrasoft pseudopotentials to the projector augmented-wave method[J]. Physical Review B, 1999, 59(3): 1758.
45. Heyd J, Peralta J E, Scuseria G E, et al. Energy band gaps and lattice parameters evaluated with the Heyd-Scuseria-Ernzerhof screened hybrid functional[J]. The Journal of Chemical Physics, 2005, 123(17): 174101.
46. Tell B, Shay J L, Kasper H M. Some properties of $AgAlTe_2$, $AgGaTe_2$, and $AgInTe_2$ [J]. Physical Review B, 1974, 9(12): 5203-5208.
47. Monkhorst H J, Pack J D. Special points for Brillouin-zone integrations[J]. Physical review B, 1976, 13(12): 5188-5192.
48. Maintz S, Deringer V L, Tchougréeff A L, et al. Analytic projection from plane-wave and PAW wavefunctions and application to chemical-bonding analysis in solids[J]. Journal of Computational Chemistry, 2013, 34(29): 2557-2567.
49. Dronskowski R, Bloechl P E. Crystal orbital Hamilton populations (COHP): energy-resolved visualization of chemical bonding in solids based on density-functional calculations[J]. The Journal of Physical Chemistry, 1993, 97(33): 8617-8624.

50. Kotochigova S, Levine Z H, Shirley E L, et al. Local-density-functional calculations of the energy of atoms[J]. Physical Review A, 1997, 55(1): 191-199.
51. Gai Y, Li J, Li S S, et al. Design of narrow-gap TiO_2: a passivated codoping approach for enhanced photoelectrochemical activity[J]. Physical Review Letters, 2009, 102(3): 036402.
52. Luque A, Martí A, Antolín E, et al. Intermediate bands versus levels in non-radiative recombination[J]. Physica B: Condensed Matter, 2006, 382(1): 320-327.
53. Zhang S B, Wei S H, Zunger A. Intrinsic n-type versus p-type doping asymmetry and the defect physics of ZnO[J]. Physical Review B, 2001, 63(7): 075205.
54. Chandrasekharaiah M S, Margrave J L. Enthalpies of formation of solid silicon dichalcogenides[J]. Journal of Physical and Chemical Reference Data, 1994, 23(3): 499-507.
55. Tomaszkiewicz I, Hope G A, O'Hare P A G. Thermochemistry of (germanium+ tellurium): I. Standard molar enthalpy of formation $\Delta_f H_m^\circ$ at the temperature 298.15 K of crystalline germanium monotelluride GeTe by fluorine-bomb calorimetry. A critical assessment of the thermodynamic properties of GeTe (cr and g) and $GeTe_2$ (g)[J]. The Journal of Chemical Thermodynamics, 1995, 27(8): 901-919.
56. Colin R, Drowart J. Thermodynamic study of tin selenide and tin telluride using a mass spectrometer[J]. Transactions of the Faraday Society, 1964, 60: 673-683.
57. Fritze S, Dadgar A, Witte H, et al. High Si and Ge n-type doping of GaN doping-Limits and impact on stress[J]. Applied Physics Letters, 2012, 100(12): 122104.
58. Zeng H, Duan G, Li Y, et al. Blue luminescence of ZnO nanoparticles based on non-equilibrium processes: defect origins and emission controls[J]. Advanced Functional Materials, 2010, 20(4): 561-572.